High-Resolution Inkjet Printing of Quantum Dot Light-Emitting Microdiode Arrays

Peihua Yang, Long Zhang, Dong Jin Kang, Robert Strahl, and Tobias Kraus*

The direct printing of microscale quantum dot light-emitting diodes (QLEDs) is a cost-effective alternative to the placement of pre-formed LEDs. The quality of printed QLEDs currently is limited by nonuniformities in droplet formation, wetting, and drying during inkjet printing. Here, optimal ink formulation which can suppress nonuniformities at the pixel and array levels is demonstrated. A solvent mixture is used to tune the ejected droplet size, ensure wetting, and provoke Marangoni flows that prevent coffee stain rings. Arrays of green QLED devices are printed at a resolution of 500 pixels in.$^{-1}$ with a maximum luminance of $\approx$3000 cd m^{-2} and a peak current efficiency of 2.8 cd A^{-1}. The resulting array quality is sufficient to print displays at state-of-the-art resolutions.

1. Introduction

Displays are indispensable components of electronic systems.[1,2] Recent "micro-LED displays" are based on arrays of small, inorganic semiconductor light-emitting diodes (micro-LEDs).[3–5] Such displays can be fabricated from diced LED microchips via transfer printing processes to obtain passive- or active-matrix micro-LED displays.[6] Micro-LED displays bring the stability and brightness of inorganic semiconductors to higher-resolution displays, but the necessity of handling micro-scale semiconductor components implies fabrication challenges and limits flexibility in display design. An alternative route is the printing of quantum dot light-emitting diodes (QLEDs) from particle dispersion: quantum dots (QDs) that individually emit light are deposited in suitable stacks in order to create displays.[7–13] The QDs are composed of inorganic semiconductors and thus potentially more stable and brighter than organic semiconductors.

Printing light-emitting devices from liquid dispersions of nanoparticles is an elegant way to bring the active component

Dr. P. Yang, L. Zhang, Dr. D. J. Kang, R. Strahl, Prof. T. Kraus
INM – Leibniz Institute for New Materials
Campus D2 2, 66123 Saarbrücken, Germany
E-mail: tobias.kraus@leibniz-inm.de
Prof. T. Kraus
Department of Colloid and Interface Chemistry
Saarland University
66123 Saarbrücken, Germany

into the devices without the challenges of pick-and-place at small scales.[14–16] It introduces challenges of its own, however, and the printing of QDs at sufficiently high resolutions with overall good emission quality is difficult.[17] Kim et al. fabricated a high-resolution QD array using electro-hydrodynamic jet printing, but the process requires high potential differences between substrate and nozzle and has limited stability and repeatability.[18] Choi et al. used an intaglio transfer printing technique to create QLED arrays where they first spin-coated onto a stamp and then transferred a part of the QDs onto the device.[19]

Inkjet printing is a widely available, comparatively straightforward technique that is material-effective and can form individual pixels and is very flexible in the design of the printed device.[20–27] Jiang et al. printed a full-color QLED display with a pixel density of 120 pixels per inch (ppi) using a commercial piezo print head and reported a maximum brightness of 400 cd m^{-2}.[28] The main challenge in high-resolution inkjet printing is to generate single ultra-small and stable droplets that dry into uniform pixels. Some groups have used pixel pockets or bank structures that confine the QD inks on the surface and prevent the merging of pixels.[21]
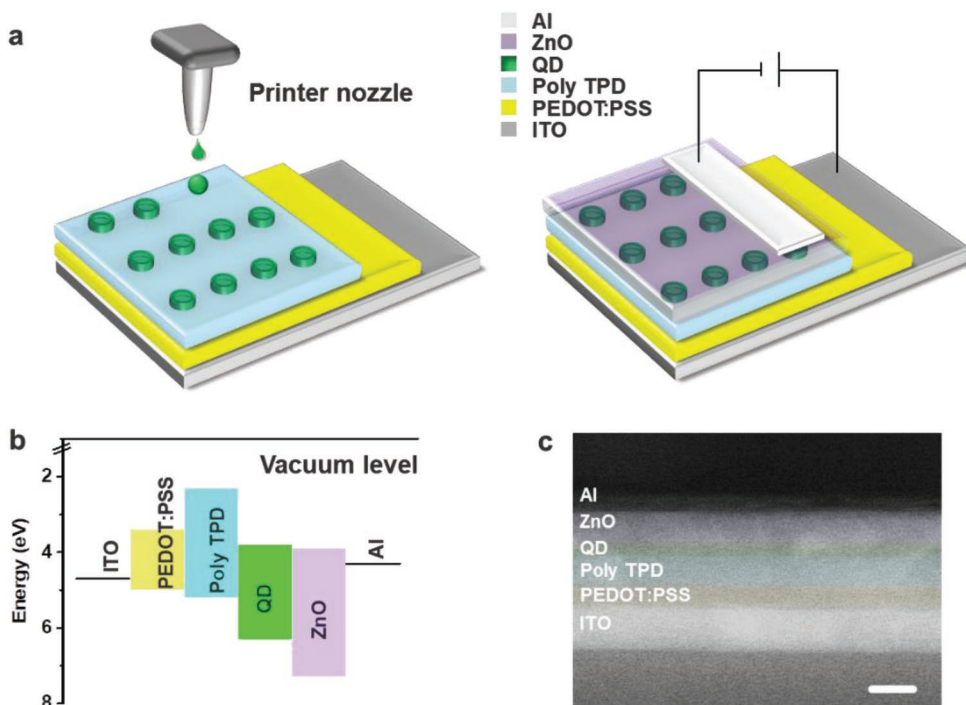
We believe that ink design is an important aspect of high-resolution QLED inkjet printing that deserves greater attention. In this contribution, we show that inks based on mixtures of octane and cyclohexylbenzene (CHB) can improve the attainable pixel quality. We systematically varied the mixing ratio in order to minimize the size of the deposited pixels at maximal areal fraction and uniform pixel flatness. We achieved a minimal pixel diameter of 20 μm for a 2 pL droplet that enables a resolution of 1000 ppi. Devices were fabricated at 500 ppi with 4 pL droplets in order to demonstrate functional QLED displays that emitted green light at a maximum luminance of $\approx$3000 cd m^{-2} at a peak current efficiency of 2.8 cd A^{-1}.

2. Results and Discussion

The inkjet printing of QDs in this work is illustrated in **Figure 1**a. Drops of QD ink were directly deposited from a piezo-driven print head on the hole transport layer, then covered with ZnO nanoparticles, and contacted with aluminum. The overall device stack thus encompassed indium tin oxide (ITO, 100 nm), poly(ethylenedioxythiophene):polystyrene sulfonate (PEDOT:PSS, 50 nm), poly(N,N'-bis(4-butylphenyl)-N,N'-bisphenylbenzidine) (poly TPD, 60 nm), QDs (25 nm), ZnO nanoparticles (80 nm), and aluminum (Al, 50 nm). Figure 1b shows the energy level diagram and highlights the conduction band matching between

ADVANCED
SCIENCE NEWS
www.advancedsciencenews.com

ADVANCED
OPTICAL
MATERIALS
www.advopticalmat.de

Figure 1. Inkjet-printing of QLED pixels. a) Schematic stack of the full device containing the inkjet-printed pixels. b) Energy level diagram. c) Cross-sectional scanning electron micrograph of the stack (scale bar: 100 nm).

Al, ZnO, and QDs that ensured efficient electron injection. The valence band offset between QDs and ZnO helped to confine the holes injected from poly TPD in the QD layer.

The goal of this work was to print high-resolution, uniformly emitting pixel arrays based on QDs. We used inks that contained the nanoparticles in mixed solvents to tune the drying process of the printed droplet and achieve uniform pixels.[29] Viscosity, density, and surface tension of the ink were adjusted via the ratio of CHB and octane (Figure S1 and Table S1, Supporting Information) while retaining a constant QD concentration of 5 mg mL^{-1} in order to create small, stable, and separated droplets that form uniform and flat pixels. Changing ink composition affected different relevant mechanisms in pixel formation that are discussed in the following.

The inverse Ohnesorge number Z is defined as the ratio of the Reynolds number (Re) and the square root of the Weber number (We)[30,31]

$$Re = \frac{\rho v d}{\eta} \tag{1}$$

$$We = \frac{\rho v^2 d}{\gamma} \tag{2}$$

$$Z = \frac{Re}{\sqrt{We}} = \frac{\sqrt{\gamma \rho d}}{\eta} \tag{3}$$

A value of $1 < Z < 10$ is required to create stable, separated droplets.[32] Note that Z only depends on ink surface tension (γ), density (ρ), viscosity (η), and nozzle diameter (d), but not on the droplet velocity (v). We found that inks containing 5 vol% octane and 95 vol% CHB exhibited nonlinear viscosity–shear

relations as shown in **Figure 2**a, which is equivalent to a viscosity of 2.06 mPa s in the inkjet process.

The velocity of the droplets depends on the waveform used to drive the piezo print head (Figure S2 and Table S2, Supporting Information). We adjusted this voltage profile in order to minimize droplet size and prevent satellites. Figure 2c shows the motion trace of a 4 pL droplet during one jetting cycle (Video S1, Supporting Information). The velocity of the droplet ranged between 4 and 8 m s^{-1} as shown in the Re–We plot in Figure 2d and corresponded to a Z value of approximately 8 that is adequate for high-resolution printing. The contact angle (CA, θ) of the ink on poly TPD depended on the solvent ratio, too, and changed from 11° to 14° (Figure 2b and Figure S1, Supporting Information), a range that has been found suitable for high-resolution printing previously.[33] Any of the solvent ratios evaluated here provided sufficient wetting of the poly TPD layer.

High-quality displays require homogenous pixels that emit toward the viewer. The shape of the dry, printed pixels depends on nanoparticles transport during drying. Sessile droplets with pure CHB as solvent exhibited the well-known capillary flow of liquid toward the edge of the droplets, which transported the QDs from the liquid volume toward the edge and resulted in a circle known as "coffee stain ring."[34] In drying droplets that contained mixed solvents, Marangoni flows toward the center were superimposed (**Figure 3**a) and weakened the coffee ring effect.[35] The relative effect of the two flows can be expressed using the ratio f of a characteristic solvent evaporation time, τ_e, and a characteristic time for QD motion, τ_q[36,37]

$$f = \frac{\tau_q}{\tau_e} \propto \frac{\eta}{\theta} \tag{4}$$
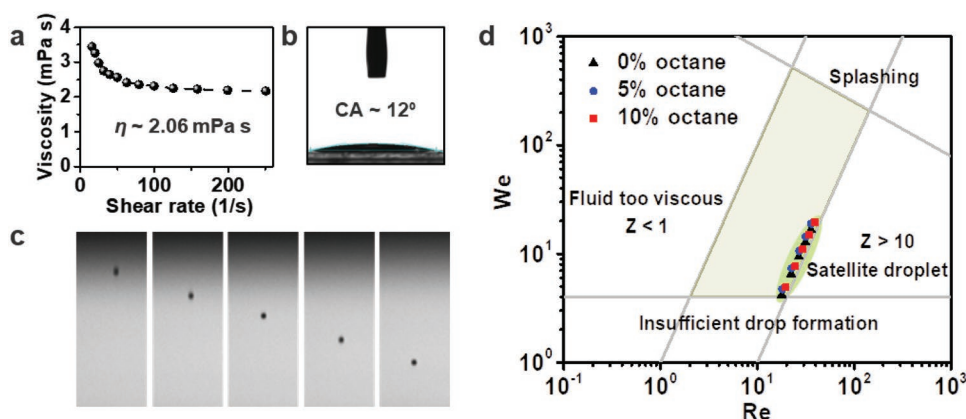
Figure 2. QD inks properties. a) Viscosity of the ink with 5% octane and b) CA of the ink on a poly TPD substrate. c) One jetting cycle of a 4 pL droplet during a time interval of 20 μs. d) A parameter map of the Reynolds and Weber numbers for inks with different octane fractions. Note that all formulations were in the (marked) range that is suitable for printing.

Large f indicates reduced coffee ring formation and uniform deposition across the pixel. We found pronounced coffee stain rings for inks with pure CHB (Figure S3, Supporting Information). Increasing octane content reduced the ring until the value of η/θ was saturating at 5% octane, resulting in a nearly uniform distribution of the QD across the pixel (Figure 3b). Larger octane fractions led to the formation of QD aggregates that were deposited at the pixel center.

We analyzed the morphology of individual pixels at the optimal octane fraction of 5% across the printed arrays by atomic force microscope (AFM). Figure 3d shows that given

suitable printing conditions, highly circular pixels were deposited. The average circularity of the pixels was above 0.92 (Figure S3, Supporting Information). The cross-sectional profile of the AFM image in Figure 3e indicates a constant thickness of approximately 25 nm with no detectable accumulation at the border. We also checked the scanning electron microscope (SEM) images of the printed QD arrays (Figure S4, Supporting Information), showing a uniform distribution and identifying with the photoluminescence (PL) microscopic images.

Inkjet print heads deposit a defined density of droplets per unit length ("dots per inch," dpi) while they are moving over the
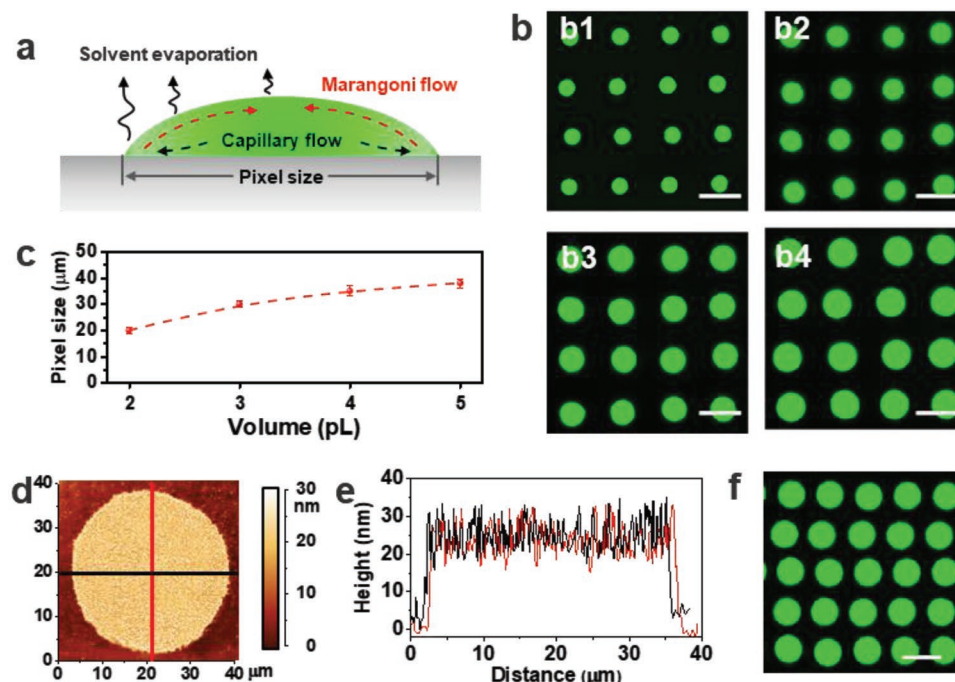
Figure 3. Printing of pixel arrays by deposition of single inkjet droplets. a) Schematic illustration of the printed pixel drying process. b) PL micrographs of pixels formed with droplet volumes from b1) 2 pL to b4) 5 pL at a constant density of 400 ppi (scale bar: 50 μm). c) Pixel size as a function of droplet volume. d) AFM image of a pixel formed from a 4 pL droplet. e) Cross-sectional height profile of the pixel shown in (d). f) Pixel array from 4 pL droplet printed at 500 ppi (scale bar: 50 μm).

substrate. Ideally, each deposited droplet forms a single pixel, so that the density of the resulting display (ppi) is identical to the dpi setting of the printer. In practice, however, droplets may fuse and reduce the true pixel density. The degree of this deviation is a function of the wetting properties and the precision of the printer (inaccurate droplet positions increase the risk of overlapping droplets). Figure 3b shows PL micrographs of pixels that were formed by printing droplets with different volumes at a fixed resolution of 400 ppi. Droplets having volumes of 2–5 pL led to circular pixels with diameters increasing from 20 to 38 µm with standard deviations below 5% over 10 by 10 pixels arrays (Figure 3c and Figure S5, Supporting Information). The pixels diameter deviations may come from the volume dissimilarity of the jetting droplets, which is controlled by piezoelectric pulse signals. These pixels are small enough to obtain a pattern resolution as high as 500–1000 ppi for a spacing of one quarter of a pixel diameter between adjacent pixels (Figure S6, Supporting Information). Note that this spacing is below the single spacing often used in literature, thus increasing the pixel density and display brightness.[19] Pixel sizes below 20 µm are very difficult to attain in inkjet printing without ink banks.[38–41] We believe that we have reached the limits attainable with conventional inkjet printing.

It is insufficient to print pixels at high resolution. The luminance of the display, an important quality parameter, is proportional to the areal fraction of the pixel. We therefore evaluated how densely we could print while retaining clear separation between the individual pixels. The theoretical density of 4 pL droplets without overlap was 580 ppi, and when we further increased the pixel density to 600 ppi, droplets merged (Figure S7, Supporting Information) and degraded the pixel array. A practical, realistic density for high areal fraction pixels was 500 ppi, as demonstrated in Figure 3f, giving an area fraction of 44%, which is near the geometric limit for a square circle array (Equation (S3), Supporting Information). We found that the fluctuations in the pixels' positions were mainly caused by slight deviations of the droplet's trajectories from the surface normal (visible in stroboscopic image series shown in Figure S2, Supporting Information). This is partially caused during droplet formation and can be reduced by optimizing the waveform, as we did, but there is a contribution from mechanical tolerances of the overall system that we did not change here; we note in passing that previous publications on inkjet-printed pixels reported similar deviations.[42,43] Specialized high-precision inkjet printers are commercially available that provide reduced tolerances and will further improve the deviations. The resolution and density that we reached are sufficient to print a 25 in. display with 8 K (8000 × 4500 pixels) resolution, sufficient for applications in displays in vehicles, for scientific visualization, geospatial imagery, and tele-immersion, for example.[44]

The printed pixel arrays were spin-coated with a ZnO electron transport layer and contacted using a sputtered Al cathode in order to create functional emitting devices. **Figure 4**a displays the electroluminescence (EL) spectrum of a 500 ppi array with a peak emission wavelength of 548 nm and a full-width at half-maximum of 33 nm. The red-shift of the PL spectrum as compared to the original QD dispersion may be caused by Förster resonant energy transfer between the densely packed QDs.[45] The emitted green light corresponds to a color coordinate of

(0.32, 0.66) in the chromaticity diagram of the Commission Internationale de l'Eclairage (CIE) in Figure 4b, which is close to the color-saturated green emission specified for high definition television (HDTV) applications.

Most applications call for bright displays with a sufficient luminance (directed light emission per area) of the printed pixels. Figure 4c shows the current density–voltage and luminance–voltage characteristics of the printed device. The turn-on voltage was about 6 V (1 cd m^{-2}), and the maximal luminance was 3050 cd m^{-2}, approximately half of that found for non-patterned, spin-coated devices, and as expected for the areal fraction occupied by pixels (Figure S8, Supporting Information). We measured luminous intensities of up to 2.8 cd A^{-1} at a luminance of 3000 cd m^{-2}, which corresponds to a maximal external quantum efficiency (EQE) of 2.4% (Figure 4d). This shows that high-resolution inkjet printing is a feasible route to efficient QD displays (a comparison to existing devices can be found in Table S3, Supporting Information).[28,37,46–53] As a digital patterning technology, inkjet printing gives rapid access to a wide range of geometries (Figure 4e) as required for rapid prototyping, personalized devices, or 3D architectures with integrated displays. Here, we successfully demonstrated the high-resolution inkjet printing of green CdSe QDs devices, and we believe that the experimental strategy and printing technical route can be adapted for other appropriate CdSe QDs and even perovskite QDs.[54,55]

3. Conclusions

In conclusion, we developed new QD inks and used them to print high-resolution QLED arrays using single droplet inkjet printing with standard printheads. The rheology and interfacial energy of the ink were tuned in order to eject small, uniform droplets, induce Marangoni flows that flattened the pixels during drying, and provide wetting properties suitable for large area fractions at high resolutions. This yielded high-quality pixel arrays at 500 ppi, which is sufficient for the standardized 8 K display type on a 25 in. panel. The strategy is not limited to green QDs; inks based on QDs with different emission colors can be inkjet printed to create RGB displays. It is compatible with flexible and soft substrates. We believe that our method can be extended to high-resolution full-color QLED displays and diversify the design of emerging flexible and wearable electronic devices.

4. Experimental Section

Materials: CdSe/ZnS core–shell type QDs (Catalog No. 748056, fluorescence λ_{em} 540 nm), zinc acetate dihydrate (99%), tetramethylammonium hydroxide pentahydrate (TMAH, 97%), dimethyl sulfoxide (DMSO, 99.8%), ethyl acetate (EA, 99.8%), CHB (97%), ethanolamine (98%), and chlorobenzene (99.8%) were purchased from Sigma-Aldrich; *n*-octane was from Acros (99+%); pixelated ITO-coated glass (Order Code S101, 20 Ω sq^{-1}), poly TPD (M521), and PEDOT:PSS (AI 4083, M121) were from Ossila.

Synthesis of ZnO Nanoparticles:[56,57] Zinc acetate dihydrate (3 mmol) was dissolved in DMSO (30 mL) and TMAH (5.5 mmol) was dissolved in ethanol (10 mL), then mixed together and stirred for 24 h under ambient conditions. An excess of EA was added in the mixture, then centrifuged
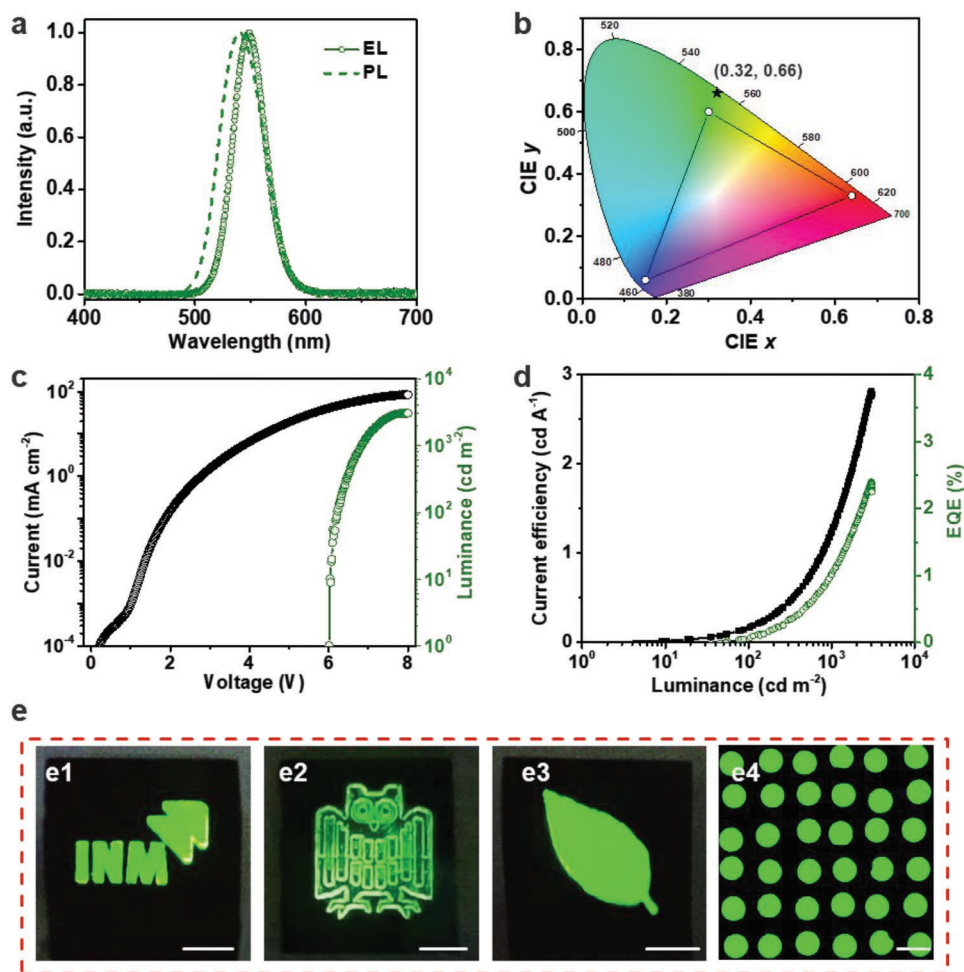
Figure 4. Performance of inkjet-printed devices. a) EL spectrum of the device and PL spectrum of the QD ink. b) The CIE coordinates of the printed pixels (star) together with HDTV color standards (circles). c) Current density and luminance versus driving voltage characteristics for the printed device. d) Current efficiency and EQE versus luminance for the device. e) Panels (e1) to (e3) show photographs of printed logos composed of pixels that demonstrate the versatility of inkjet printing. (Scale bars: 5 mm.) Panel (e4) shows micrographs of the emitting pixels. (Scale bar: 50 μm.)

and re-dispersed the precipitate in ethanol at a concentration of 20 mg mL^{-1} with the addition of 160 μL ethanolamine. ZnO nanoparticles were filtered with a 0.2 μm polytetrafluoroethylene filter before use. The transmission electron microscopy (TEM) image showed the synthesized ZnO nanoparticles had an average diameter of 5 nm (Figure S9, Supporting Information).

QLED Device Fabrication: Pixelated ITO-coated glass substrates were cleaned by ultrasonication in acetone, ethanol, and deionized (DI) water. The substrates were dried by nitrogen stream and subjected to 30 min of oxygen plasma treatment to enhance the hydrophilicity of the surface. PEDOT:PSS solutions (AI 4083, filtered through a 0.2 μm filter) were spin-coated onto the ITO-coated glass substrates at 4000 rpm for 60 s and baked at 150 °C for 30 min. Hole transport material poly TPD (8 mg mL^{-1} in chlorobenzene) was sequentially spin-coated on the PEDOT:PSS layer at 2000 rpm for 30 s and then heated at 150 °C for 30 min. The inkjet printing of QD layer on substrates was accomplished by using a PiXDRO LP50 printer equipped with a 9 μm diameter inkjet nozzle at room temperature (≈25 °C). Here, an inert cartridge (liquid crystal polymer) was used to store the ink, and the ink concentration was about 5 mg mL^{-1} in different solvents. For the spin-coated QD film, QD solution (5 mg mL^{-1} in octane) was spin-coated on the substrate at 2000 rpm for 30 s and heated at 70 °C for 30 min. Pre-filtered ZnO nanoparticles

(20 mg mL^{-1}) were subsequently spin-coated at 2000 rpm for 60 s and then the device was transferred to argon glove box with annealing at 150 °C for 30 min. All the solution processes were carried out in ambient environment except for the ZnO annealing process. Finally, the substrates were transferred to a vacuum chamber at 2×10^{-5} Torr to deposit aluminum cathode (50 nm). The devices were encapsulated by the cover glasses using UV-curable resin.

Characterizations: SEM image was performed with a Quanta 400 SEM (FEI, Germany). TEM image was recorded using a JEM 2010 (JEOL, Germany). The viscosity of the inks was recorded by Discovery Hybrid Rheometer (HR-3). The CA and surface tension were measured by DataPhysics Instrument GmbH (OCA 35). The fluorescent microscopy images were recorded by Zeiss Polscope Observer. PL spectrum of QD ink was measured with a fluorescence spectrophotometer (FluoroMax-3, HORIBA Scientific). The printed pixels' sizes and their circularity were obtained by analyzing PL images of arrays with 10 by 10 pixels using the ImageJ software. AFM images were acquired in the tapping mode using a NanoWizard3 machine (JPK Instruments, Germany). A Keithley 2450 electrometer was employed for current density–voltage characterizations, an Ocean Optics sphere (ISP-30-6-I) coupled with a Flame Miniature Spectrometer (calibrated by a HL-3 plus standard light source) were used for light output measurements. The effective area of the device was ≈4 mm^2 for the electrical and luminous measurements.

1901429 (5 of 7)

[1] H.-W. Chen, J.-H. Lee, B.-Y. Lin, S. Chen, S.-T. Wu, *Light: Sci. Appl.* **2018**, *7*, 17168.

[2] H.-Y. Gao, Q.-X. Yao, P. Liu, Z.-Q. Zheng, J.-C. Liu, H.-D. Zheng, C. Zeng, Y.-J. Yu, T. Sun, Z.-X. Zeng, *Chin. Phys. B* **2016**, *25*, 094203.

[3] M. Malinverni, D. Martin, N. Grandjean, *Appl. Phys. Lett.* **2015**, *107*, 051107.

[4] H. E. Lee, D. Lee, T.-I. Lee, J. H. Shin, G.-M. Choi, C. Kim, S. H. Lee, J. H. Lee, Y. H. Kim, S.-M. Kang, S. H. Park, I.-S. Kang, T.-S. Kim, B.-S. Bae, K. J. Lee, *Nano Energy* **2019**, *55*, 454.

[5] H. E. Lee, J. H. Shin, J. H. Park, S. K. Hong, S. H. Park, S. H. Lee, J. H. Lee, I.-S. Kang, K. J. Lee, *Adv. Funct. Mater.* **2019**, *29*, 1808075.

[6] R. S. Cok, M. Meitl, R. Rotzoll, G. Melnik, A. Fecioru, A. J. Trindade, B. Raymond, S. Bonafede, D. Gomez, T. Moore, C. Prevatte, E. Radauscher, S. Goodwin, P. Hines, C. A. Bower, *J. Soc. Inf. Disp.* **2017**, *25*, 589.

[7] Y. E. Panfil, M. Oded, U. Banin, *Angew. Chem., Int. Ed.* **2018**, *57*, 4274.

[8] H. Shen, Q. Gao, Y. Zhang, Y. Lin, Q. Lin, Z. Li, L. Chen, Z. Zeng, X. Li, Y. Jia, S. Wang, Z. Du, L. S. Li, Z. Zhang, *Nat. Photonics* **2019**, *13*, 192.

[9] H. Moon, C. Lee, W. Lee, J. Kim, H. Chae, *Adv. Mater.* **2019**, *31*, 1804294.

[10] Q. Shan, J. Li, J. Song, Y. Zou, L. Xu, J. Xue, Y. Dong, C. Huo, J. Chen, B. Han, H. Zeng, *J. Mater. Chem. C* **2017**, *5*, 4565.

[11] X. Yang, Z.-H. Zhang, T. Ding, N. Wang, G. Chen, C. Dang, H. V. Demir, X. W. Sun, *Nano Energy* **2018**, *46*, 229.

[12] M. K. Choi, J. Yang, D. C. Kim, Z. Dai, J. Kim, H. Seung, V. S. Kale, S. J. Sung, C. R. Park, N. Lu, T. Hyeon, D.-H. Kim, *Adv. Mater.* **2018**, *30*, 1703279.

[13] Y. Fang, K. Ding, Z. Wu, H. Chen, W. Li, S. Zhao, Y. Zhang, L. Wang, J. Zhou, B. Hu, *ACS Nano* **2016**, *10*, 10023.

[14] J. Feng, X. Yan, Y. Zhang, X. Wang, Y. Wu, B. Su, H. Fu, L. Jiang, *Adv. Mater.* **2016**, *28*, 3732.

[15] J. Feng, X. Jiang, X. Yan, Y. Wu, B. Su, H. Fu, J. Yao, L. Jiang, *Adv. Mater.* **2017**, *29*, 1603652.

[16] J. Feng, W. Wen, X. Wei, X. Jiang, M. Cao, X. Wang, X. Zhang, L. Jiang, Y. Wu, *Adv. Mater.* **2019**, *31*, 1807880.

[17] J. Hou, M. Li, Y. Song, *Angew. Chem., Int. Ed.* **2018**, *57*, 2544.

[18] B. H. Kim, M. S. Onses, J. B. Lim, S. Nam, N. Oh, H. Kim, K. J. Yu, J. W. Lee, J.-H. Kim, S.-K. Kang, C. H. Lee, J. Lee, J. H. Shin, N. H. Kim, C. Leal, M. Shim, J. A. Rogers, *Nano Lett.* **2015**, *15*, 969.

[19] M. K. Choi, J. Yang, K. Kang, D. C. Kim, C. Choi, C. Park, S. J. Kim, S. I. Chae, T.-H. Kim, J. H. Kim, T. Hyeon, D.-H. Kim, *Nat. Commun.* **2015**, *6*, 7149.

[20] Z. Cui, *Printed Electronics: Materials, Technologies and Applications*, Higher Education Press, John Wiley & Sons, Singapore **2016**.

[21] L. Lan, J. Zou, C. Jiang, B. Liu, L. Wang, J. Peng, *Front. Optoelectron.* **2017**, *10*, 329.

[22] W. Huang, M. Xu, J. Liu, J. Wang, Y. Zhu, J. Liu, H. Rong, J. Zhang, *Adv. Funct. Mater.* **2019**, *29*, 1808762.

[23] J. Zimmermann, L. Porcarelli, T. Rödlmeier, A. Sanchez-Sanchez, D. Mecerreyes, G. Hernandez-Sosa, *Adv. Funct. Mater.* **2018**, *28*, 1705795.

[24] X. Peng, J. Yuan, S. Shen, M. Gao, A. S. R. Chesman, H. Yin, J. Cheng, Q. Zhang, D. Angmo, *Adv. Funct. Mater.* **2017**, *27*, 1703704.

[25] Y. Chu, Y. Qian, P. Chahal, C. Cao, *Adv. Sci.* **2019**, *6*, 1801653.

[26] Z. Gu, K. Wang, H. Li, M. Gao, L. Li, M. Kuang, Y. S. Zhao, M. Li, Y. Song, *Small* **2017**, *13*, 1603217.

[27] L. Xie, X. Xiong, Q. Chang, X. Chen, C. Wei, X. Li, M. Zhang, W. Su, Z. Cui, *Small* **2019**, *15*, 1900111.

[28] C. Jiang, L. Mu, J. Zou, Z. He, Z. Zhong, L. Wang, M. Xu, J. Wang, J. Peng, Y. Cao, *Sci. China: Chem.* **2017**, *60*, 1349.

[29] R. G. Larson, *AIChE J.* **2014**, *60*, 1538.

[30] D. McManus, S. Vranic, F. Withers, V. Sanchez-Romaguera, M. Macucci, H. Yang, R. Sorrentino, K. Parvez, S.-K. Son, G. Iannaccone, K. Kostarelos, C. Casiraghi, G. Fiori, *Nat. Nanotechnol.* **2017**, *12*, 343.

[31] B. Derby, *Engineering* **2015**, *1*, 113.

[32] Y. Liu, B. Derby, *Phys. Fluids* **2019**, *31*, 032004.

[33] W. Zapka, *Handbook of Industrial Inkjet Printing: A Full System Approach*, Wiley-VCH, Weinheim **2017**.

[34] R. D. Deegan, O. Bakajin, T. F. Dupont, G. Huber, S. R. Nagel, T. A. Witten, *Nature* **1997**, *389*, 827.

[35] H. Hu, R. G. Larson, *J. Phys. Chem. B* **2006**, *110*, 7090.

[36] X. Shen, C.-M. Ho, T.-S. Wong, *J. Phys. Chem. B* **2010**, *114*, 5269.

[37] C. Jiang, Z. Zhong, B. Liu, Z. He, J. Zou, L. Wang, J. Wang, J. Peng, Y. Cao, *ACS Appl. Mater. Interfaces* **2016**, *8*, 26162.

[38] H. Sirringhaus, T. Kawase, R. H. Friend, T. Shimoda, M. Inbasekaran, W. Wu, E. P. Woo, *Science* **2000**, *290*, 2123.

[39] B. Derby, *Annu. Rev. Mater. Res.* **2010**, *40*, 395.

[40] W. Wu, *Nanoscale* **2017**, *9*, 7342.

[41] W. Scheideler, V. Subramanian, *Nanotechnology* **2019**, *30*, 272001.

[42] C.-H. Tien, C.-H. Hung, T.-H. Yu, *J. Disp. Technol.* **2009**, *5*, 147.

[43] D. Lee, D. Lee, Y. Won, H. Hong, Y. Kim, H. Song, J. C. Pyun, Y. S. Cho, W. Ryu, J. Moon, *Small* **2016**, *12*, 1446.

[44] N. Tao, G. S. Schmidt, O. G. Staadt, M. A. Livingston, R. Ball, R. May, in *IEEE Virtual Reality Conf. (VR 2006)*, IEEE, Piscataway, NJ **2006**, p. 223.

[45] X. Dai, Y. Deng, X. Peng, Y. Jin, *Adv. Mater.* **2017**, *29*, 1607022.

[46] T. R. Hebner, C. C. Wu, D. Marcy, M. H. Lu, J. C. Sturm, *Appl. Phys. Lett.* **1998**, *72*, 519.

[47] H. Kobayashi, S. Kanbe, S. Seki, H. Kigchi, M. Kimura, I. Yudasaka, S. Miyashita, T. Shimoda, C. R. Towns, J. H. Burroughes, R. H. Friend, *Synth. Met.* **2000**, *111–112*, 125.

[48] T. Gohda, Y. Kobayashi, K. Okano, S. Inoue, K. Okamoto, S. Hashimoto, E. Yamamoto, H. Morita, S. Mitsui, M. Koden, *SID Symp. Dig. Tech. Pap.* **2006**, *37*, 1767.

[49] H. M. Haverinen, R. A. Myllylä, G. E. Jabbour, *Appl. Phys. Lett.* **2009**, *94*, 073108.

[50] V. Wood, M. J. Panzer, J. Chen, M. S. Bradley, J. E. Halpert, M. G. Bawendi, V. Bulović, *Adv. Mater.* **2009**, *21*, 2151.

[51] J. Han, D. Ko, M. Park, J. Roh, H. Jung, Y. Lee, Y. Kwon, J. Sohn, W. K. Bae, B. D. Chin, C. Lee, *J. Soc. Inf. Disp.* **2016**, *24*, 545.

**ADVANCED
SCIENCE NEWS**

www.advancedsciencenews.com

**ADVANCED
OPTICAL
MATERIALS**

www.advopticalmat.de

[52] Y. Liu, F. Li, Z. Xu, C. Zheng, T. Guo, X. Xie, L. Qian, D. Fu, X. Yan, *ACS Appl. Mater. Interfaces* **2017**, *9*, 25506.

[53] Y. Liu, F. Li, X. Xie, W. Chen, Z. Xu, C. Zheng, H. Hu, T. Guo, *SID Symp. Dig. Techn. Pap.* **2017**, *48*, 1715.

[54] L. Shi, L. Meng, F. Jiang, Y. Ge, F. Li, X.-G. Wu, H. Zhong, *Adv. Funct. Mater.* **2019**, *29*, 1903648.

[55] M. Zhu, Y. Duan, N. Liu, H. Li, J. Li, P. Du, Z. Tan, G. Niu, L. Gao, Y. Huang, Z. Yin, J. Tang, *Adv. Funct. Mater.* **2019**, *29*, 1903294.

[56] X. Dai, Z. Zhang, Y. Jin, Y. Niu, H. Cao, X. Liang, L. Chen, J. Wang, X. Peng, *Nature* **2014**, *515*, 96.

[57] K. Ding, Y. Fang, S. Dong, H. Chen, B. Luo, K. Jiang, H. Gu, L. Fan, S. Liu, B. Hu, L. Wang, *Adv. Opt. Mater.* **2018**, *6*, 1800347.